

Nonclassical dynamics of Néel vector and magnetization accompanied by THz and high-harmonic radiation from ultrafast-light-driven NiO antiferromagnet insulator

Federico Garcia-Gaitan,¹ Adrian E. Feiguin,² and Branislav K. Nikolić^{1,*}

¹*Department of Physics and Astronomy, University of Delaware, Newark DE 19716, USA*

²*Department of Physics, Northeastern University, Boston, MA 02115, USA*

Ultrafast-light-driven strongly correlated antiferromagnetic insulators, such as prototypical NiO with large energy gap $\simeq 4$ eV, have recently attracted experimental attention using photons of both *above-gap* [K. Gillmeister *et al.*, Nat. Commun. **11**, 4095 (2020)] and *subgap* [H. Qiu *et al.*, Nat. Phys. **17**, 388 (2021)] energy. In the latter context, also of great interest to applications, emission of THz radiation is also observed from NiO/Pt bilayers, where heavy metal (HM) Pt introduces strong spin-orbit coupling (SOC). However, in contrast to amply studied spintronic THz emitters using fs laser pulse (fsLP)-driven FM/HM (FM-ferromagnetic metal of conventional type, such as Fe, Ni, Co) bilayers, where ultrafast demagnetization takes place and is directly related to THz emission, microscopic mechanisms of electromagnetic (EM) radiation from NiO/HM bilayer remain obscure as total magnetization of NiO is *zero* prior to fsLP application. Here we employ the two-orbital Hubbard-Hund-Heisenberg model and study, via numerically exact quantum many-body methods, the dynamics of its Néel vector and *nonequilibrium* magnetization. This reveals *nonclassical* (i.e., not describable by Landau-Lifshitz equation) dynamics of Néel vector and nonequilibrium magnetization, changing *only* in length while not rotating, where the former is substantially reduced in the case above-gap fsLP. Additionally, we compute EM radiation by time-dependence of magnetization, as well as of local charge currents, finding that both contributions are significant in THz frequency range *only* in NiO with proximity SOC introduced by HM layer. Above THz range, we find integer high-harmonic generation, as well as unusual *noninteger* harmonics for above-gap fsLP pump.

Introduction.—Pump-probe experiments [1] on strongly correlated antiferromagnetic (AF) insulators (AFI), like prototypical NiO, have revealed [2] intricate fundamental effects, such as coherent long-lived many-body dynamics resulting from a coupling to the AF background where coherent oscillations persists on surprisingly long timescales ~ 2 ps. The fs laser pulse (fsLP) in these experiments has a central frequency that is *above-gap* between two Hubbard bands [Fig. 2], as it has also been typically the focus of theoretical studies [2, 3]. Theoretical interest also exists to understand quantum tunneling, multiphoton absorption and the so-called “Keldysh crossover” and the ensuing nonlinear doublon-holon pair production in the case of *subgap* fsLP pump [4–7]. These findings comprise a panoply of fundamental effects that cannot be found in fsLP-driven conventional band insulators and semiconductors.

The same NiO material driven by subgap fsLP, but in combination with heavy metal (HM) layer (like Pt,W,Ta) introducing effects [8] due to strong spin-orbit coupling (SOC), have been very recently explored [9, 10] as spintronic THz emitter [11–16]. Isolated ferromagnetic metal (FM) layers (such as Co,Fe,Ni) or FM/HM bilayers have been intensely studied for nearly 30 years in order to understand ultrafast demagnetization [17, 18], as well as THz emission by these systems, which is much stronger in the case of bilayers [11–15, 19] than in the case of a single FM layer [14, 19, 20]. The fsLP in spintronic experiments typically has a central wavelength of $\simeq 800$ nm, so that its photons have energy centered around $\hbar\Omega_0 \simeq 1.55$ eV which is *subgap* [9, 10, 21] with respect to the separation $\simeq 4$ eV between the two Hubbard bands

of NiO. The spintronic phenomena in such experiments on subgap-fsLP-excited NiO have been interpreted [9, 10] by borrowing the standard intuitive picture [11–15, 19] (for its recent modifications, however, via microscopic theory see Refs. [22–24]) developed for FM/HM bilayers. That is, an ultrafast spin current is somehow generated that flows from NiO into the HM layer, so that latter can convert it into charge current via the inverse spin Hall effect [25]. The time-dependent charge current is needed to obtain sizable electromagnetic (EM) radiation in the far-field (FF) region [Fig. 1], as well as to interpret [9, 10] the enhancement [14] of the emitted radiation when switching from FM to FM/HM systems. This is because magnetic dipole radiation [14, 19, 20] from time-dependent magnetization $\mathbf{M}(t)$ is $1/c$ smaller [22] than radiation by a time-dependent charge current. However, this picture does not explain the microscopic mechanism that generates the assumed spin current in NiO/HM bilayers (only speculation exist thus far [26]), or why the frequency spectrum of such current has features within 0.1–3 THz range that is imprinted in the EM radiation detected experimentally [9, 10]. It is obvious that fsLP will drive electrons into dynamics at its own center frequency Ω_0 , as well as at *integer* (typically odd [27, 28]) multiples of Ω_0 for sufficiently intense fsLP. Such high-harmonic generation (HHG) in current and EM radiation has been vigorously explored in recent years in diverse quantum materials [29, 30], including strongly correlated ones [6, 7, 27, 31, 32]. Finally, it remains unclear what type of dynamics is obeyed by the Néel vector (as the difference of two sublattices magnetizations) and magnetization (as the sum of sublattice magnetizations,

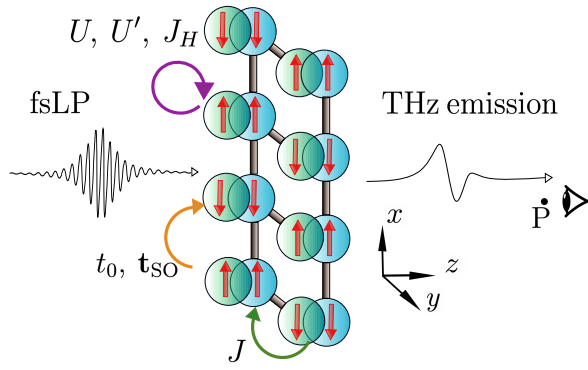


FIG. 1. Schematic view of two-orbitals-per-site 2HHH model [2] for NiO on a ladder geometry. It can also include additional Rashba SOC [8, 36], introduced through t_{SO} spin-dependent matrix [37] hoppings, and arising from proximity effects [8, 38–41] in NiO/HM bilayers employed experimentally [9, 10]. Other denoted parameters, describing local Coulomb and (U and U') Hund interactions (J_H), Heisenberg exchange interaction (J), and electron hopping (t_0) between sites, are explained in Eqs. (1)–(4). This setup is driven out of equilibrium by fsLP, and we compute EM radiation emitted by it in *both* THz and HHG frequency range.

which is necessarily a nonequilibrium quantity because $\mathbf{M}(t=0) \equiv 0$, when compared to standard demagnetization [14, 17, 18] of FM layers, where magnetization vector shrinks. In the case of thin FM layers, a rapid and straightforward analysis of the direction of $\mathbf{M}(t)$ and its magnitude is achieved via [14] magneto-optical Kerr or Faraday effects. In contrast, they do not apply to AFs, so novel ideas have been explored [33] to detect the presumed [10, 34, 35] rotation of the Néel vector.

Thus, developing a microscopic understanding of the response of AFI to subgap fsLP (that is, by starting from a suitable quantum many-body Hamiltonian and using tools of nonequilibrium quantum statistical mechanics), would also help to resolve a number of outstanding issues in AF optospintrronics [42]. Note that, specifically for NiO which is a strongly correlated material sharing features of both Mott and charge-transfer insulators [2, 43], X-ray techniques applied as a probe after subgap fsLP pump have revealed [21] possible substantial [1, 3] changes of its electronic structure, such as emergence of midgap states and Hubbard gap reduction persisting on time scales > 2 ps. Such phenomena originating from charge dynamics must be taken into account together with local spin dynamics, as they can lead to *inextricable* complex spin-charge dynamics [2, 44]. In the case of weakly correlated FMs, proper description of spin-charge dynamics is achieved via time-dependent density functional theory (TDDFT) which has provided [45–49] a most detailed insight into a sequence of fast changing events [50] and their effect [22, 23] on THz emission. However, application [51] of TDDFT to NiO is impeded

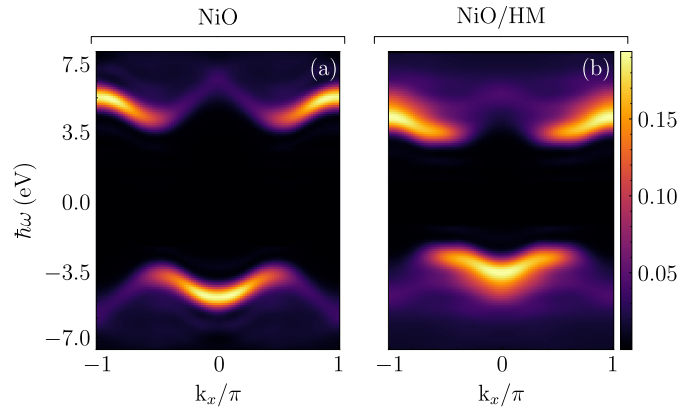


FIG. 2. The tDMRG-computed [55, 56] spectral function [57] of Hubbard model on a ladder [Fig. 1] for: (a) plain NiO; and (b) NiO with proximity induced Rashba SOC due to adjacent HM layer within NiO/HM bilayer employed in THz spintronics experiments [9, 10]. Here we focus on the bonding symmetry sector by choosing $k_y = 0$ [56].

by intricacies in including a time-dependent [52, 53] Hubbard U to properly capture a strong on-site Coulomb interaction that is also dynamical (as opposed to static U in conventional equilibrium DFT+U [54] calculations).

In this Letter, we aim to capture all the essential physics of strongly correlated electrons within NiO, in the presence of fsLP and SOC, by employing a two-orbital Hubbard-Hund-Heisenberg (2HHH) model [2] and by simulating its time evolution via numerically exact quantum-many body methods. Its ground AF state is formed by local spins $S = 1$ [58] at each site, that are composed of two elemental spins $s = 1/2$ located on two orbitals at that site [Fig. 1], with Hund interaction included between them in order to achieve fixed and stable S per atom [59, 60]. In addition, to take into account adjacent nonmagnetic HM layer in THz spintronics experiments [9, 10], we also include SOC of the Rashba type [8, 36] into the 2HHH model of Ref. [2]. Thus, the introduced SOC models proximity effects [8, 38–41] around the NiO/HM interface, that modifies the electronic structure on the NiO side due to the HM layer (NiO, in turn, modifies bands of HM layer, but we do not include HM layer explicitly due to high computational expense). This model is placed onto a ladder geometry [Fig. 1], allowing for its spectral function [55–57] to be computed via numerically (quasi)exact simulations using time-dependent density matrix renormalization group (tDMRG) [61–64] applicable to quasi-one-dimensional lattices. We complement the study with an additional set of numerical simulations using massively parallel exact diagonalization (ED) methods [65] for Hubbard-type systems, implemented within the HΦ package [66, 67]. This technique allows us to access longer times (required for THz radiation calculations) than those possible via tensor network algorithms (like tDMRG) encountering “entangle-

ment barrier" [68, 69].

By considering a multi-orbital ladder, spin-charge separation is largely suppressed, so a plethora of dissipative mechanisms based on electron-spin interaction become active, such as the AF background interaction with doublons and holons [2, 70] or local dissipation caused by the Hund interaction [71–73]. Our principal results, revealing highly nonclassical dynamics of Néel vector and nonequilibrium magnetization, and the ensuing radiation at both high harmonics of fsLP and in much lower THz range, are given in Figs. 3 and 4. Prior to discussing these results, we introduce useful concepts and notations.

Model and Methods.—The monolayer [74] of NiO is modeled on a tight-binding ladder [Fig. 1] with two orbitals per site hosting Ni only, while O atom is not modeled explicitly albeit O-mediated interactions are included. The same 2HHH model, but without any SOC, was used in Ref. [2] where above-gap pumping of NiO by fsLP was studied experimentally and theoretically. Our Hamiltonian, $\hat{H} = \hat{H}_{\text{local}} + \hat{H}_{\text{ex}} + \hat{H}_{\text{TB}} + \hat{H}_{\text{SOC}}$, is built on top of the model from Ref. [2] by including possible Rashba SOC [8, 36] to describe the NiO/HM bilayer used in THz spintronic experiments [9, 10]. The local terms of \hat{H}_{local} account for the Hubbard and Hund physics

$$\begin{aligned} \hat{H}_{\text{local}} = & U \sum_{i,\alpha} \hat{n}_{i,\alpha\uparrow} \hat{n}_{i,\alpha\downarrow} - \mu \sum_{i,\alpha,\sigma} \hat{n}_{i\alpha\sigma} - g\mu_B B_z^{\text{imp}} \hat{s}_{1\alpha}^z \\ & + \sum_{i,\alpha<\beta} \sum_{\sigma,\sigma'} (U' - J_H \delta_{\sigma\sigma'}) \hat{n}_{i\alpha\sigma} \hat{n}_{i\beta\sigma'} \\ & + \gamma J_H \sum_{i,\alpha \neq \beta} \left(\hat{c}_{i\alpha\uparrow}^\dagger \hat{c}_{i\alpha\downarrow}^\dagger \hat{c}_{i\beta\downarrow} \hat{c}_{i\beta\uparrow} + \text{H.c.} \right) \\ & + \gamma J_H \sum_{i,\alpha \neq \beta} \left(\hat{c}_{i\alpha\uparrow}^\dagger \hat{c}_{i\beta\downarrow}^\dagger \hat{c}_{i\alpha\downarrow} \hat{c}_{i\beta\uparrow} + \text{H.c.} \right). \end{aligned} \quad (1)$$

Here $\hat{c}_{i\alpha\sigma}$ ($\hat{c}_{i\alpha\sigma}^\dagger$) is the creation (annihilation) operator of an electron of spin $\sigma = \uparrow, \downarrow$ in orbital $\alpha = 1, 2$ located at site i ; $\hat{n}_{i\alpha\sigma}$ is the corresponding number operator; U , U' , and J_H are the intra-orbital Coulomb, inter-orbital Coulomb, and inter-orbital (or Hund [59, 60]) exchange interaction, respectively; μ is the onsite chemical potential; and B_z^{imp} is a magnetic field added [75] on site $i = 1$ to lift the degeneracy between spin- \uparrow and spin- \downarrow electrons. The Heisenberg exchange interaction between spins at nearest neighbor (NN) sites is given by

$$\hat{H}_{\text{ex}} = \sum_{\langle ij \rangle, \alpha} \left[J \left(\hat{s}_{i\alpha}^x \cdot \hat{s}_{j\alpha}^x + \hat{s}_{i\alpha}^y \cdot \hat{s}_{j\alpha}^y \right) + J_z \hat{s}_{i\alpha}^z \cdot \hat{s}_{j\alpha}^z \right], \quad (2)$$

where $\langle ij \rangle$ denotes summation over the NN sites; $\hat{s}_{i\alpha}^p = \sum_{\sigma,\sigma'} \hat{c}_{i\alpha\sigma}^\dagger \frac{1}{2} \hat{\sigma}_{\sigma\sigma'}^p \hat{c}_{i\alpha\sigma'}$ is the electron spin operator expressed using $\hat{\sigma}^p$ as one of three ($p = x, y, z$) Pauli matrices; and $J = J_z = 0.1$ eV in the isotropic case. The kinetic term in tight-binding (TB) Hamiltonian

$$\hat{H}_{\text{TB}} = -t_0 \sum_{\langle ij \rangle, \alpha, \sigma} \left(\hat{c}_{i\alpha\sigma}^\dagger \hat{c}_{j\alpha\sigma} + \text{H.c.} \right), \quad (3)$$

where t_0 is the hopping parameter. An additional TB term is employed to introduce proximity SOC—switched off in NiO case and switched on in NiO/HM case in Figs. 3 and 4—as given by

$$\hat{H}_{\text{SOC}} = \sum_{\langle ij \rangle, \alpha} \left(\hat{\mathbf{c}}_{i\alpha}^\dagger \mathbf{t}_{\text{SO}} \hat{\mathbf{c}}_{j\alpha} + \text{H.c.} \right), \quad (4)$$

where $\hat{\mathbf{c}}_{i\alpha}^\dagger = (\hat{c}_{i\alpha\uparrow}^\dagger \quad \hat{c}_{i\alpha\downarrow}^\dagger)$ denotes row vector of two creation operators and \mathbf{t}_{SO} is a direction-dependent 2×2 matrix hopping [37] with values $-it_{\text{SO}} \hat{\sigma}_y (it_{\text{SO}} \hat{\sigma}_x)$ for horizontal (vertical) bonds. The \hat{H}_{SOC} term is of the Rashba type [36], assumed to originate from proximity to HM layer employed experimentally [9, 10], as found in DFT calculations on FM/HM [8] of AFI/HM [40] bilayers. Realistic parameters values for NiO are taken from prior first-principles calculations for strongly correlated electrons [76], such as from DFT+U [54] and/or DFT+dynamical mean field theory [77, 78] studies: $U \approx 8$ eV; $t_0 \approx 1$ eV; $J_H \approx 1$ eV; and we set $U' = U - 2J_H$ and $\gamma = 1$ for symmetry reasons [71]. Half-filling is selected by setting the chemical potential to $\mu = (3U - 5J_H)/2$ [2]. The magnetic field at site 1, $g\mu_B B_z^{\text{imp}} = 0.1$ eV, as generated by, e.g., a static impurity, induces [75] Néel "checkerboard" order $\langle \hat{S}_i^z \rangle = -\langle \hat{S}_j^z \rangle \neq 0$ (i and j are two NN sites) in the ground state (GS). Nevertheless, the GS in our simulations retains nonzero entanglement, as witnessed in many recent experiments even at finite temperature [79, 80], so it is not identical to unentangled Néel ket $|\uparrow\downarrow \dots \uparrow\downarrow\rangle$.

The fsLP is introduced via its vector potential [gray line in Figs. 3(e) and 4(e)] of amplitude A_{max} , which couples to electrons in the form of a Peierls phase [81, 82] multiplying hoppings in Eqs. (3) and (4) by a factor

$$P = \exp \left[iz_{\text{max}} e^{-\frac{(t-t_p)^2}{2\sigma_{\text{light}}^2}} \cos(\Omega_0 t) \right],$$
 so $t_0(t) = Pt_0$ and $\mathbf{t}_{\text{SO}}(t) = P\mathbf{t}_{\text{SO}}$. Here $z_{\text{max}} = ea_0 A_{\text{max}}/\hbar = 0.2$ is the dimensionless parameter [83] quantifying the fsLP intensity; a_0 is the lattice constant; and $\sigma_{\text{light}} = 20$ fs determines the width of the Gaussian envelope which is initially centered at $t_p = 200$ fs. The center frequency of the fsLP is either $\hbar\Omega_0 = 1.55$ eV in Fig. 3, corresponding to a subgap 800 nm wavelength commonly employed in THz spintronic experiments [9–15, 19]; or $\hbar\Omega_0 = 8$ eV in Fig. 4 for above-gap fsLP [gaps are shown in Fig. 2]. The electric field of the fsLP is linearly polarized along the xy -direction (i.e., diagonal to the ladder) in Fig. 1. The time evolution described by $\hat{H}(t)$ on a 4×2 ladder is obtained via ED [65] by means of the HΦ package [66, 67], where the GS was found using the Lanczos algorithm and the evolution operator is computed via a Taylor expansion considering up to 15 terms. The time step was chosen as $\delta t = 0.005\hbar/t_0$.

To compute the EM radiation generated by the charge dynamics, the expectation value $I_{ij} \equiv \langle \hat{I}_{ij} \rangle$ of the bond charge current operator [37],

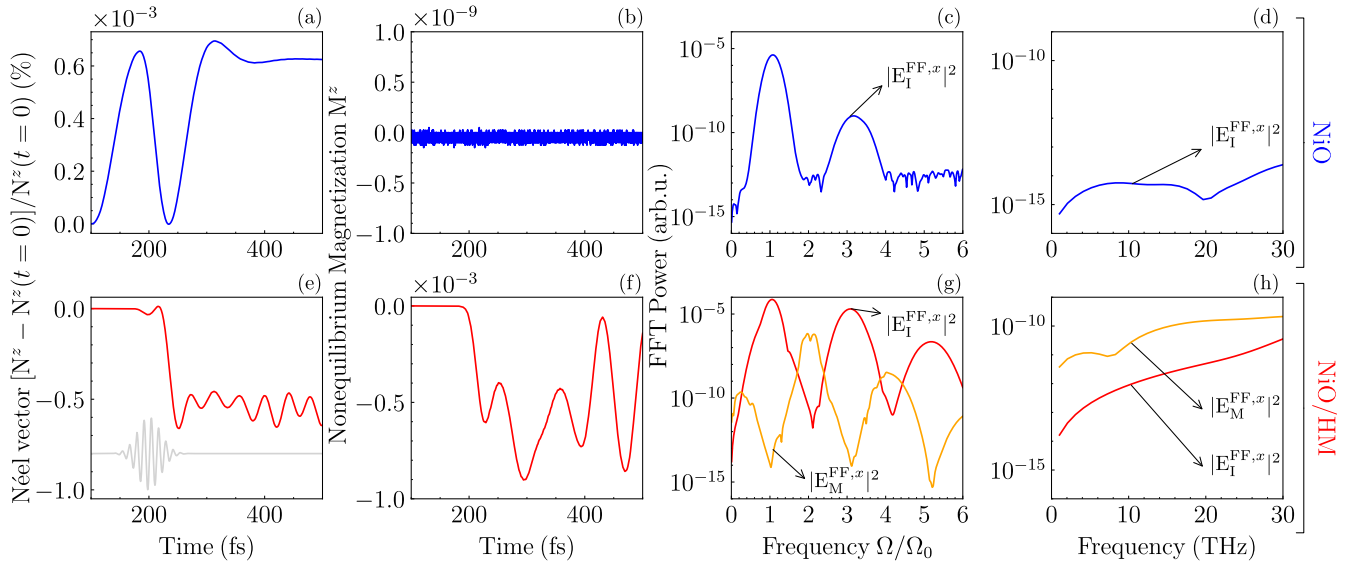


FIG. 3. Time dependence, initiated by a fsLP with *subgap* central frequency, of: (a),(e) Néel vector; and (b),(f) nonequilibrium magnetization. (c),(d),(g),(h) Fast Fourier transform (FFT) power spectrum—within (c),(g) HHG frequencies or or (d),(h) THz frequencies—of the *x*-component of electric field of EM radiation emitted by the dynamics of magnetization [Eq. (5)] or bond charge currents [Eq. (5)]. The top row of panels is for plain NiO, while the bottom row is for NiO assumed to contain [8] the Rashba SOC due to proximity effects [38–41] from HM layer within NiO/HM bilayer studied in recent experiments [9, 10].

$\hat{I}_{ij} = \frac{ie}{\hbar} \sum_{\alpha} [\hat{\mathbf{c}}_{i\alpha}^\dagger \{t_0(t)\hat{\sigma}_0 + \mathbf{t}_{\text{SO}}(t)\} \hat{\mathbf{c}}_{j\alpha} - \text{H.c.}]$ from site i to site j with $\hat{\sigma}_0$ being a unit 2×2 matrix, is plugged [24, 84, 85] into the Jefimenko formula [86] for the electric field

$$\mathbf{E}_I^{\text{FF}}(\mathbf{r}, t) = \frac{1}{4\pi\epsilon_0 c^2} \sum_{P_{i \rightarrow j}=1}^{N_b} \int_{P_{i \rightarrow j}} \left[(\mathbf{r} - \mathbf{l}) \frac{\partial_t I_{ij}(t_r)}{|\mathbf{r} - \mathbf{l}|^3} (\mathbf{r} - \mathbf{l}) \cdot \mathbf{e}_x - \frac{\partial_t I_{ij}(t_r)}{|\mathbf{r} - \mathbf{l}|} \mathbf{e}_x \right] dl.$$

The most general Jefimenko formula [86], as proper solution of the Maxwell equations [87], is reorganized [88] above in order to isolate the FF contributions decaying as $\sim 1/r$. We compute radiation at point P in Fig. 1 which is at a distance $100a_0$ away from NiO. Here, $t_r = t - |\mathbf{r} - \mathbf{l}|/c$ emphasizes retardation due to relativistic causality; bond currents are assumed to be homogeneous [24, 84, 85] along the path $P_{i \rightarrow j}$ from site i to site j of length dl ; N_b is the number of bonds; and we use shorthand notation $\partial_t \equiv \partial/\partial_t$. In addition, we also compute the electric field of FF radiation by magnetic dipole, i.e., due to the time-dependence of the nonequilibrium magnetization

$$\mathbf{E}_M^{\text{FF}}(\mathbf{r}, t) = \frac{1}{4\pi\epsilon_0 c^3} \sum_i \frac{\mathbf{r} - \mathbf{l}_i}{|\mathbf{r} - \mathbf{l}_i|^2} \times \partial_t^2 \mathbf{M}_i(t_r), \quad (6)$$

where \mathbf{l}_i indicates the location of site i . Time-dependent magnetization $M^z(t)$ and Néel vector $N^z(t)$ are obtained by summing spin expectation values at each site, $M^z = \sum_i M_i^z = \sum_{i,\alpha} \langle \hat{s}_{i\alpha}^z \rangle(t)$ and $N^z = \sum_i N_i^z \sum_{i,\alpha} (-1)^i \langle \hat{s}_{i\alpha}^z \rangle(t)$, where a “snake-like”

enumeration of ladder sites is assumed. Note that other (the *x*- and *y*-components) are vanishingly small.

Results and Discussion.—The usual first take at interpreting experiments on subgap light-driven AFIs, including NiO [10, 89, 90], invokes [89–92] a direct coupling of light magnetic field (or an effective one due to inverse Faraday [90] or inverse Cotton-Mouton [10] effects) to local magnetization of AFIs. This leads to classical dynamics of the Néel vector, which rotates without changing its length [10], in accord with phenomenological theories [34, 35] of Landau-Lifshitz (LL) type [93]. However, limitations of this approach are often found in experiments [90, 94], which is not surprising as light-charge coupling is much stronger [46], so electrons should be explicitly included. But the picture of classical LL dynamics [10, 34, 35] is appealing because it is difficult to develop intuition on how electrons of AFI, with gapped energy spectrum [Fig. 2], absorb subgap light and then affect its magnetic ordering. In case of AF metals, it is easy to envisage (and calculate [85]) how that fsLP generates photocurrent of conduction electrons, which are then spin-polarized by the magnetic background and exert spin torque [85] onto local magnetization. Its dynamics follows (for weak-intensity fsLP to avoid demagnetization [17, 18]) classical LL dynamics (valid at sufficiently high temperature and for AFIs with $S > 1$ [69]). For AFIs, there is no such shortcut and one has to handle complexities of photoexcited Hubbard model [3–7], which cannot [95], in general, be reduced to studying just their final outcome on magnetic order.

Indeed, our quantum many-body calculations for sub-

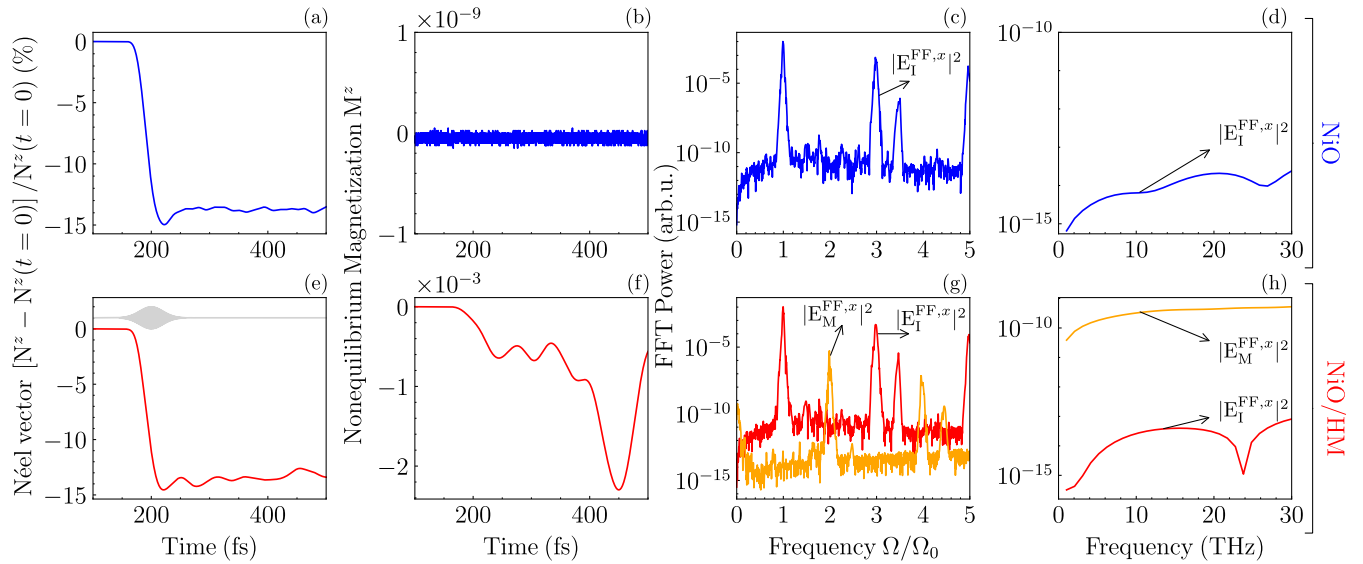


FIG. 4. The same information as in Fig. 3, but using fsLP whose central frequency of $\hbar\Omega_0 = 8$ eV is *above-gap* of Fig. 2.

gap fsLP-driven NiO reveal highly *nonclassical* [75, 96] (i.e., outside any description by LL-type theories [10, 34]) dynamics of the Néel vector and magnetization in Fig. 3. That is, both vectors are changing length along the z -axis (orthogonal to the ladder in Fig. 1) while *not rotating* at all. Nonequilibrium magnetization remains zero in plain NiO [Fig. 3(b)]. However, $M^z(t) \neq 0$ in SO-proximitized NiO [Fig. 3(f)], which is akin to experimentally observed [97] weak ferromagnetism in photodoped Mott insulator with native SOC. The nonzero $\partial_t^2 M^z(t_r)$ emits magnetic dipole [Eq. (6)] THz radiation [orange line in Fig. 3(h)], which can (surprisingly, when compared to FM layers [22]) surpass the contribution from $\partial_t I_{ij}(t_r)$ [red curve in Fig. 3(h)]. Importantly, THz emission from both of these two sources is significant *only* when proximity SOC is present in NiO/HM bilayer [Fig. 3(h)], in full accord with experiments [9, 10]. Thus, our theory explains these experiments without invoking qualitative speculations [9, 10, 26], while showing that concepts borrowed from FM/HM systems (like interlayer spin current and spin-to-charge conversion within HM [11, 12, 14, 15, 19, 23]) are not necessary for THz emission from AFI. The magnetic dipole radiation exhibits even integer HHG [Fig. 3(g)], while odd ones are expected [27] for radiation from $\partial_t I_{ij}(t_r)$, as dictated by symmetry-imposed selection rules of Floquet group theory [98]. Although SOC breaks inversion symmetry, odd integer HHG is preserved [28, 99]. This offers a scheme—*detect even HHG in EM radiation from AFI*—which directly corroborates how magnetization dynamics in magnets driven by fsLP can be much faster [48, 100] than observed in low-energy transport experiments [26].

For above-gap fsLP in Fig. 4, we find reduction of Néel vector by up to 15%, signifying suppression [3] of AF or

der in the GS. This is in sharp contrast to its minuscule change for subgap fsLP in Fig. 3. Similarly to subgap fsLP, nonequilibrium magnetization [Fig. 4(f)] emerges *only* when proximity SOC is switched on. Unlike the subgap fsLP case, charge current and its THz radiation are not significantly enhanced by including proximity SOC [Fig. 4(d) vs. Fig. 4(h)]. The selection rules for HHG remain the same, allowing only odd integer HHG of $E_I^{\text{FF},x}$ [Fig. 4(c),(g)] and even ones of $E_M^{\text{FF},x}$ [Fig. 4(g)]. Curiously, we also find *noninteger* HHG of both $E_I^{\text{FF},x}$ and $E_M^{\text{FF},x}$, which are beyond standard Floquet theory and its selection rules [98]. Theoretical [27] and experimental [30] reports of noninteger HHG are scarce, and their understanding is in its infancy. For example, they could arise [27] from correlation-driven population of multiple Floquet states (unlike population of a single state used in Floquet group theory [98]), whose exploration we relegate to future studies.

F.G-G. and B.K.N. were supported by the US National Science Foundation (NSF) through the University of Delaware Materials Research Science and Engineering Center, DMR-2011824. The supercomputing time was provided by DARWIN (Delaware Advanced Research Workforce and Innovation Network), which is supported by NSF Grant No. MRI-1919839. A.E.F. was supported by the US Department of Energy, Office of Basic Energy Sciences under Grant No. DE-SC0022311.

* bnikolic@udel.edu

[1] Y. Wang, M. Claassen, C. D. Pemmaraju, C. Jia, B. Moritz, and T. P. Devereaux, Theoretical under-

standing of photon spectroscopies in correlated materials in and out of equilibrium, *Nat. Rev. Mater.* **3**, 312 (2018).

[2] K. Gillmeister, D. Golež, C.-T. Chiang, N. Bittner, Y. Pavlyukh, J. Berakdar, P. Werner, and W. Widdra, Ultrafast coupled charge and spin dynamics in strongly correlated NiO, *Nat. Commun.* **11**, 4095 (2020).

[3] Y. Wang, M. Claassen, B. Moritz, and T. P. Devereaux, Producing coherent excitations in pumped Mott antiferromagnetic insulators, *Phys. Rev. B* **96**, 235142 (2017).

[4] T. Oka, Nonlinear doublon production in a Mott insulator: Landau-Dykne method applied to an integrable model, *Phys. Rev. B* **86**, 075148 (2012).

[5] K. Shinjo, S. Sota, and T. Tohyama, Glassy dynamics of the one-dimensional Mott insulator excited by a strong terahertz pulse, *Phys. Rev. Res.* **4**, L032019 (2022).

[6] Y. Murakami, M. Eckstein, and P. Werner, High-harmonic generation in Mott insulators, *Phys. Rev. Lett.* **121**, 057405 (2018).

[7] Y. Murakami, S. Takayoshi, A. Koga, and P. Werner, High-harmonic generation in one-dimensional Mott insulators, *Phys. Rev. B* **103**, 035110 (2021).

[8] S. Grytsyuk, A. Belabbes, P. M. Haney, H.-W. Lee, K.-J. Lee, M. D. Stiles, U. Schwingenschlögl, and A. Manchon, k -asymmetric spin splitting at the interface between transition metal ferromagnets and heavy metals, *Phys. Rev. B* **93**, 174421 (2016).

[9] H. Qiu, L. Zhou, C. Zhang, J. Wu, Y. Tian, S. Cheng, S. Mi, H. Zhao, Q. Zhang, D. Wu, *et al.*, Ultrafast spin current generated from an antiferromagnet, *Nat. Phys.* **17**, 388 (2021).

[10] E. Rongione, O. Gueckstock, M. Mattern, O. Gomonay, H. Meer, C. Schmitt, R. Ramos, T. Kikkawa, M. Mičica, E. Saitoh, *et al.*, Emission of coherent thz magnons in an antiferromagnetic insulator triggered by ultrafast spin-phonon interactions, *Nat. Commun.* **14**, 1818 (2023).

[11] T. Seifert, S. Jaiswal, U. Martens, J. Hannegan, L. Braun, P. Maldonado, F. Freimuth, A. Kronenberg, J. Henrizi, I. Radu, *et al.*, Efficient metallic spintronic emitters of ultrabroadband terahertz radiation, *Nat. Photonics* **10**, 483 (2016).

[12] Y. Wu, M. Elyasi, X. Qiu, M. Chen, Y. Liu, L. Ke, and H. Yang, High-performance THz emitters based on ferromagnetic/nonmagnetic heterostructures, *Adv. Mater.* **29**, 1603031 (2017).

[13] M. B. Jungfleisch, Q. Zhang, W. Zhang, J. E. Pearson, R. D. Schaller, H. Wen, and A. Hoffmann, Control of terahertz emission by ultrafast spin-charge current conversion at Rashba interfaces, *Phys. Rev. Lett.* **120**, 207207 (2018).

[14] R. Rouzegar, L. Brandt, L. c. v. Nádvorník, D. A. Reiss, A. L. Chekhov, O. Gueckstock, C. In, M. Wolf, T. S. Seifert, W. Brouwer, *et al.*, Laser-induced terahertz spin transport in magnetic nanostructures arises from the same force as ultrafast demagnetization, *Phys. Rev. B* **106**, 144427 (2022).

[15] T. S. Seifert, D. Go, H. Hayashi, R. Rouzegar, F. Freimuth, K. Ando, Y. Mokrousov, and T. Kampfrath, Time-domain observation of ballistic orbital-angular-momentum currents with giant relaxation length in tungsten, *Nat. Nanotechnol.* **18**, 1132 (2023).

[16] A. Leitenstorfer, A. S. Moskalenko, T. Kampfrath, J. Kono, E. Castro-Camus, K. Peng, N. Qureshi, D. Turchinovich, K. Tanaka, A. G. Markelz, *et al.*, The 2023 terahertz science and technology roadmap, *J. Phys. D* **56**, 223001 (2023).

[17] E. Beaurepaire, J.-C. Merle, A. Daunois, and J.-Y. Bigot, Ultrafast spin dynamics in ferromagnetic nickel, *Phys. Rev. Lett.* **76**, 4250 (1996).

[18] X. Chen, R. Adam, D. E. Bürgler, F. Wang, Z. Lu, L. Pan, S. Heidtfeld, C. Greb, M. Liu, Q. Liu, J. Wang, C. M. Schneider, and D. Cao, Ultrafast demagnetization in ferromagnetic materials: Origins and progress, *Phys. Rep.* **1102**, 1 (2025).

[19] Y. Liu, H. Cheng, Y. Xu, P. Vallobra, S. Eimer, X. Zhang, X. Wu, T. Nie, and W. Zhao, Separation of emission mechanisms in spintronic terahertz emitters, *Phys. Rev. B* **104**, 064419 (2021).

[20] E. Beaurepaire, G. M. Turner, S. M. Harrel, M. C. Beard, J.-Y. Bigot, and C. A. Schmuttenmaer, Coherent terahertz emission from ferromagnetic films excited by femtosecond laser pulses, *Appl. Phys. Lett.* **84**, 3465 (2004).

[21] X. Wang, R. Y. Engel, I. Vaskivskyi, D. Turenne, V. Shokeen, A. Yaroslavtsev, O. Gränäs, R. Knut, J. O. Schunck, S. Dzirarhytski, *et al.*, Ultrafast manipulation of the NiO antiferromagnetic order via sub-gap optical excitation, *Faraday Discuss.* **237**, 300 (2022).

[22] A. Kefayati and B. K. Nikolić, Origins of electromagnetic radiation from spintronic terahertz emitters: A time-dependent density functional theory plus Jefimenko equations approach, *Phys. Rev. Lett.* **133**, 136704 (2024).

[23] A. Kefayati, Y. Ren, M. B. Jungfleisch, L. Gundlach, J. Q. Xiao, and B. K. Nikolić, Deciphering the origin of spin current in spintronic terahertz emitters and its imprint on their electromagnetic radiation via time-dependent density functional theory, [arXiv:2410.07360](https://arxiv.org/abs/2410.07360) (2024).

[24] J. Varela-Manjarres, A. Kefayati, M. B. Jungfleisch, J. Q. Xiao, and B. K. Nikolić, Charge and spin current pumping by ultrafast demagnetization dynamics, *Phys. Rev. B* **110**, L060410 (2024).

[25] E. Saitoh, M. Ueda, H. Miyajima, and G. Tatara, Conversion of spin current into charge current at room temperature: Inverse spin-Hall effect, *Appl. Phys. Lett.* **88**, 182509 (2006).

[26] J. Han, R. Cheng, L. Liu, H. Ohno, and S. Fukami, Coherent antiferromagnetic spintronics, *Nat. Mater.* **22**, 684 (2023).

[27] C. S. Lange, T. Hansen, and L. B. Madsen, Noninteger high-order harmonic generation from extended correlated systems, *Phys. Rev. A* **109**, 063103 (2024).

[28] N. Tancogne-Dejean, F. G. Eich, and A. Rubio, Effect of spin-orbit coupling on the high harmonics from the topological Dirac semimetal Na₃Bi, *npj Comput. Mater.* **8**, 145 (2022).

[29] S. Ghimire and D. A. Reis, High-harmonic generation from solids, *Nat. Phys.* **15**, 10 (2018).

[30] C. P. Schmid, L. Weigl, P. Grössing, V. Junk, C. Gorini, S. Schlauderer, S. Ito, M. Meierhofer, N. Hofmann, D. Afanasiev, *et al.*, Tunable non-integer high-harmonic generation in a topological insulator, *Nature* **593**, 385 (2021).

[31] S. Imai, A. Ono, and S. Ishihara, High harmonic generation in a correlated electron system, *Phys. Rev. Lett.*

124, 157404 (2020).

[32] C. Orthodoxou, A. Zaïr, and G. H. Booth, High harmonic generation in two-dimensional Mott insulators, *npj Quantum Mater.* **6**, 76 (2021).

[33] V. Saidl, P. Némec, P. Wadley, V. Hills, R. P. Campion, V. Novák, K. W. Edmonds, F. Maccherozzi, S. S. Dhesi, B. L. Gallagher, *et al.*, Optical determination of the Néel vector in a CuMnAs thin-film antiferromagnet, *Nat. Photonics* **11**, 91 (2017).

[34] E. G. Galkina and B. A. Ivanov, Phenomenological description of spin dynamics in antiferromagnets: Short history and modern development, *Low Temp. Phys.* **47**, 765 (2021).

[35] H. V. Gomonay and V. M. Loktev, Spin transfer and current-induced switching in antiferromagnets, *Phys. Rev. B* **81**, 144427 (2010).

[36] A. Manchon, H. C. Koo, J. Nitta, S. M. Frolov, and R. A. Duine, New perspectives for Rashba spin-orbit coupling, *Nat. Mater.* **14**, 871 (2015).

[37] B. K. Nikolić, L. P. Zárbo, and S. Souma, Imaging mesoscopic spin Hall flow: Spatial distribution of local spin currents and spin densities in and out of multiterminal spin-orbit coupled semiconductor nanostructures, *Phys. Rev. B* **73**, 075303 (2006).

[38] J. M. Marmolejo-Tejada, K. Dolui, P. Lazić, P.-H. Chang, S. Smidstrup, D. Stradi, K. Stokbro, and B. K. Nikolić, Proximity band structure and spin textures on both sides of topological-insulator/ferromagnetic-metal interface and their charge transport probes, *Nano Lett.* **17**, 5626 (2017).

[39] K. Dolui, U. Bajpai, and B. K. Nikolić, Effective spin-mixing conductance of topological-insulator/ferromagnet and heavy-metal/ferromagnet spin-orbit-coupled interfaces: A first-principles Floquet-nonequilibrium Green function approach, *Phys. Rev. Mater.* **4**, 121201 (2020).

[40] K. Dolui, A. Suresh, and B. K. Nikolić, Spin pumping from antiferromagnetic insulator spin-orbit-proximitized by adjacent heavy metal: a first-principles Floquet-nonequilibrium Green function study, *J. Phys. Mater.* **5**, 034002 (2022).

[41] I. Žutić, A. Matos-Abiague, B. Scharf, H. Dery, and K. Belashchenko, Proximity materials, *Mater. Today* **22**, 85 (2019).

[42] P. Némec, M. Fiebig, T. Kampfrath, and A. V. Kimel, Antiferromagnetic opto-spintronics, *Nat. Phys.* **14**, 229 (2018).

[43] F. Lechermann, W. Körner, D. F. Urban, and C. Elsässer, Interplay of charge-transfer and Mott-Hubbard physics approached by an efficient combination of self-interaction correction and dynamical mean-field theory, *Phys. Rev. B* **100**, 115125 (2019).

[44] N. Bittner, D. Golež, H. U. R. Strand, M. Eckstein, and P. Werner, Coupled charge and spin dynamics in a photoexcited doped Mott insulator, *Phys. Rev. B* **97**, 235125 (2018).

[45] K. Krieger, J. K. Dewhurst, P. Elliott, S. Sharma, and E. K. U. Gross, Laser-induced demagnetization at ultrafast time scales: Predictions of TDDFT, *J. Chem. Theory Comput.* **11**, 4870 (2015).

[46] Z. Chen and L.-W. Wang, Role of initial magnetic disorder: A time-dependent ab initio study of ultrafast demagnetization mechanisms, *Sci. Adv.* **5**, eaau8000 (2019).

[47] N. Wu, S. Zhang, D. Chen, Y. Wang, and S. Meng, Three-stage ultrafast demagnetization dynamics in a monolayer ferromagnet, *Nat. Commun.* **15**, 2804 (2024).

[48] M. S. Mrudul and P. M. Oppeneer, Ab initio investigation of laser-induced ultrafast demagnetization of $l1_0$ fept: Intensity dependence and importance of electron coherence, *Phys. Rev. B* **109**, 144418 (2024).

[49] V. Shokeen, M. Sanchez Piaia, J.-Y. Bigot, T. Müller, P. Elliott, J. K. Dewhurst, S. Sharma, and E. K. U. Gross, Spin flips versus spin transport in nonthermal electrons excited by ultrafast optical pulses in transition metals, *Phys. Rev. Lett.* **119**, 107203 (2017).

[50] P. Tengdin, W. You, C. Chen, X. Shi, D. Zusin, Y. Zhang, C. Gentry, A. Blonsky, M. Keller, P. M. Oppeneer, *et al.*, Critical behavior within 20 fs drives the out-of-equilibrium laser-induced magnetic phase transition in nickel, *Sci. Adv.* **4**, eaap9744 (2018).

[51] J. K. Dewhurst, P. Elliott, S. Shallcross, E. K. U. Gross, and S. Sharma, Laser-induced intersite spin transfer, *Nano Lett.* **18**, 1842 (2018).

[52] N. Tancogne-Dejean, M. A. Sentef, and A. Rubio, Ultrafast modification of Hubbard U in a strongly correlated material: Ab initio high-harmonic generation in NiO, *Phys. Rev. Lett.* **121**, 097402 (2018).

[53] O. K. Orhan and D. D. O'Regan, TDDFT+ U : a critical assessment of the Hubbard U correction to exchange-correlation kernels and potentials, *Phys. Rev. B* **99**, 165120 (2019).

[54] V. I. Anisimov, J. Zaanen, and O. K. Andersen, Band theory and Mott insulators: Hubbard U instead of Stoner I, *Phys. Rev. B* **44**, 943 (1991).

[55] K. Zawadzki and A. E. Feiguin, Time- and momentum-resolved tunneling spectroscopy of pump-driven nonthermal excitations in Mott insulators, *Phys. Rev. B* **100**, 195124 (2019).

[56] C. Yang and A. E. Feiguin, Spectral function of Mott-insulating Hubbard ladders: From fractionalized excitations to coherent quasiparticles, *Phys. Rev. B* **99**, 235117 (2019).

[57] G. W. Winkler, M. Ganahl, D. Schuricht, H. G. Evertz, and S. Andergassen, Interaction effects in a microscopic quantum wire model with strong spin-orbit interaction, *New J. Phys.* **19**, 063009 (2017).

[58] A. Nag, H. C. Robarts, F. Wenzel, J. Li, H. Elnaggar, R.-P. Wang, A. C. Walters, M. García-Fernández, F. M. F. de Groot, M. W. Haverkort, *et al.*, Many-body physics of single and double spin-flip excitations in NiO, *Phys. Rev. Lett.* **124**, 067202 (2020).

[59] M. Hoffmann and S. Blügel, Systematic derivation of realistic spin models for beyond-Heisenberg solids, *Phys. Rev. B* **101**, 024418 (2020).

[60] K. M. Stadler, G. Kotliar, S.-S. B. Lee, A. Weichselbaum, and J. von Delft, Differentiating Hund from Mott physics in a three-band Hubbard-Hund model: Temperature dependence of spectral, transport, and thermodynamic properties, *Phys. Rev. B* **104**, 115107 (2021).

[61] S. R. White and A. E. Feiguin, Real-time evolution using the density matrix renormalization group, *Phys. Rev. Lett.* **93**, 076401 (2004).

[62] A. J. Daley, C. Kollath, U. Schollwöck, and G. Vidal, Time-dependent density-matrix renormalization-group using adaptive effective Hilbert spaces, *J. Stat. Mech.* **2004**, P04005 (2004).

[63] P. Schmitteckert, Nonequilibrium electron transport using the density matrix renormalization group method, *Phys. Rev. B* **70**, 121302 (2004).

[64] A. E. Feiguin, The density matrix renormalization group and its time-dependent variants, *AIP Conf. Proc.* **1419**, 5 (2011).

[65] M. Innerberger, P. Worm, P. Prauhart, and A. Kauch, Electron-light interaction in nonequilibrium: exact diagonalization for time-dependent Hubbard hamiltonians, *Eur. Phys. J. Plus* **135**, 922 (2020).

[66] K. Ido, M. Kawamura, Y. Motoyama, K. Yoshimi, Y. Yamaji, S. Todo, N. Kawashima, and T. Misawa, Update of HΦ: Newly added functions and methods in versions 2 and 3, *Comput. Phys. Commun.* **298**, 109093 (2024).

[67] M. Kawamura, K. Yoshimi, T. Misawa, Y. Yamaji, S. Todo, and N. Kawashima, Quantum lattice model solver HΦ, *Comput. Phys. Commun.* **217**, 180 (2017).

[68] A. Lerose, M. Sonner, and D. A. Abanin, Overcoming the entanglement barrier in quantum many-body dynamics via space-time duality, *Phys. Rev. B* **107**, L060305 (2023).

[69] F. Garcia-Gaitan and B. K. Nikolić, Fate of entanglement in magnetism under lindbladian or non-Markovian dynamics and conditions for their transition to Landau-Lifshitz-Gilbert classical dynamics, *Phys. Rev. B* **109**, L180408 (2024).

[70] Y. Murakami, D. Golež, M. Eckstein, and P. Werner, Photo-induced nonequilibrium states in Mott insulators, *arXiv:2310.05201* (2023).

[71] J. Rincón, E. Dagotto, and A. E. Feiguin, Photoinduced Hund excitons in the breakdown of a two-orbital Mott insulator, *Phys. Rev. B* **97**, 235104 (2018).

[72] M. Lysne, Y. Murakami, and P. Werner, Signatures of bosonic excitations in high-harmonic spectra of Mott insulators, *Phys. Rev. B* **101**, 195139 (2020).

[73] H. U. R. Strand, D. Golež, M. Eckstein, and P. Werner, Hund's coupling driven photocarrier relaxation in the two-band Mott insulator, *Phys. Rev. B* **96**, 165104 (2017).

[74] We use monolayer of NiO and do not include HM layer explicitly due to high computational expense of our numerically exact calculations. Nevertheless, this limitation is not a drawback for capturing essential features of experiments as they find [10] the highest intensity of emitted THz radiation for the thinnest NiO layer driven by subgap fsLP.

[75] M. D. Petrović, P. Mondal, A. E. Feiguin, and B. K. Nikolić, Quantum spin torque driven transmutation of an antiferromagnetic Mott insulator, *Phys. Rev. Lett.* **126**, 197202 (2021).

[76] K. Held, Electronic structure calculations using dynamical mean field theory, *Adv. Phys.* **56**, 829 (2007).

[77] J. Kuneš, V. I. Anisimov, A. V. Lukoyanov, and D. Vollhardt, Local correlations and hole doping in NiO: A dynamical mean-field study, *Phys. Rev. B* **75**, 165115 (2007).

[78] L. Zhang, P. Staar, A. Kozhevnikov, Y.-P. Wang, J. Trinastic, T. Schulthess, and H.-P. Cheng, DFT + DMFT calculations of the complex band and tunneling behavior for the transition metal monoxides MnO, FeO, CoO, and NiO, *Phys. Rev. B* **100**, 035104 (2019).

[79] A. Scheie, P. Laurell, A. M. Samarakoon, B. Lake, S. E. Nagler, G. E. Granroth, S. Okamoto, G. Alvarez, and D. A. Tennant, Witnessing entanglement in quantum magnets using neutron scattering, *Phys. Rev. B* **103**, 224434 (2021).

[80] P. Laurell, A. Scheie, E. Dagotto, and D. A. Tennant, Witnessing entanglement and quantum correlations in condensed matter: A review, *arXiv:2405.10899* (2024).

[81] G. Panati, H. Spohn, and S. Teufel, Effective dynamics for Bloch electrons: Peierls substitution and beyond, *Commun. Math. Phys.* **242**, 547 (2003).

[82] J. Li, D. Golež, G. Mazza, A. J. Millis, A. Georges, and M. Eckstein, Electromagnetic coupling in tight-binding models for strongly correlated light and matter, *Phys. Rev. B* **101**, 205140 (2020).

[83] U. Bajpai, B. S. Popescu, P. Plecháč, B. K. Nikolić, L. E. F. Foa Torres, H. Ishizuka, and N. Nagaosa, Spatio-temporal dynamics of shift current quantum pumping by femtosecond light pulse, *JPhys. Materials* **2**, 025004 (2019).

[84] M. Ridley, L. Kantorovich, R. van Leeuwen, and R. Tuovinen, Quantum interference and the time-dependent radiation of nanojunctions, *Phys. Rev. B* **103**, 115439 (2021).

[85] A. Suresh and B. K. Nikolić, Quantum classical approach to spin and charge pumping and the ensuing radiation in terahertz spintronics: Example of the ultrafast light-driven weyl antiferromagnet Mn₃Sn, *Phys. Rev. B* **107**, 174421 (2023).

[86] O. D. Jefimenko, *Electricity and Magnetism* (Appleton Century-Crofts, New York, 1966).

[87] D. J. Griffiths and M. A. Heald, Time-dependent generalizations of the Biot–Savart and Coulomb laws, *Am. J. Phys.* **59**, 111 (1991).

[88] K. T. McDonald, The relation between expressions for time-dependent electromagnetic fields given by Jefimenko and by Panofsky and Phillips, *Am. J. Phys.* **65**, 1074 (1997).

[89] T. Kampfrath, A. Sell, G. Klatt, A. Pashkin, S. Mährlein, T. Dekorsy, M. Wolf, M. Fiebig, A. Leitnerstorfer, and R. Huber, Coherent terahertz control of antiferromagnetic spin waves, *Nat. Photonics* **5**, 31 (2011).

[90] T. Satoh, S.-J. Cho, R. Iida, T. Shimura, K. Kuroda, H. Ueda, Y. Ueda, B. A. Ivanov, F. Nori, and M. Fiebig, Spin oscillations in antiferromagnetic NiO triggered by circularly polarized light, *Phys. Rev. Lett.* **105**, 077402 (2010).

[91] A. V. Kimel, B. A. Ivanov, R. V. Pisarev, P. A. Usachev, A. Kirilyuk, and T. Rasing, Inertia-driven spin switching in antiferromagnets, *Nat. Phys.* **5**, 727 (2009).

[92] T. G. H. Blank, K. A. Grishunin, B. A. Ivanov, E. A. Mashkovich, D. Afanasiev, and A. V. Kimel, Empowering control of antiferromagnets by Thz-induced spin coherence, *Phys. Rev. Lett.* **131**, 096701 (2023).

[93] L. D. Landau and E. M. Lifshitz, On the theory of the dispersion of magnetic permeability in ferromagnetic bodies, *Phys. Z. Sowjetunion* **8**, 153 (1935).

[94] F. Formisano, T. T. Gareev, D. I. Khusyainov, A. E. Fedianin, R. M. Dubrovin, P. P. Syrnikov, D. Afanasiev, R. V. Pisarev, A. M. Kalashnikova, J. H. Mentink, *et al.*, Coherent THz spin dynamics in antiferromagnets beyond the approximation of the Néel vector, *APL Mater.* **12**, 011105 (2024).

[95] J. H. Mentink, K. Balzer, and M. Eckstein, Ultrafast and reversible control of the exchange interaction in Mott insulators, *Nat. Commun.* **6**, 6708 (2015).

- [96] A. Mitrofanov and S. Urazhdin, Nonclassical spin transfer effects in an antiferromagnet, *Phys. Rev. Lett.* **126**, 037203 (2021).
- [97] D. Afanasiev, A. Gatalova, D. J. Groenendijk, B. A. Ivanov, M. Gibert, S. Gariglio, J. Mentink, J. Li, N. Dasari, M. Eckstein, *et al.*, Ultrafast spin dynamics in photodoped spin-orbit Mott insulator Sr_2IrO_4 , *Phys. Rev. X* **9**, 021020 (2019).
- [98] O. Neufeld, D. Podolsky, and O. Cohen, Floquet group theory and its application to selection rules in harmonic generation, *Nat. Commun.* **10**, 405 (2019).
- [99] M. Lysne, Y. Murakami, M. Schüler, and P. Werner, High-harmonic generation in spin-orbit coupled systems, *Phys. Rev. B* **102**, 081121 (2020).
- [100] A. V. Kimel and M. Li, Writing magnetic memory with ultrashort light pulses, *Nat. Rev. Mater.* **4**, 189 (2019).